Quantitative Study of Optical Frequency Noise to Intensity Noise Conversion in Line-by-Line Pulse Shaping

Chen-Bin Huang, *Member, IEEE*, Zhi Jiang, Daniel E. Leaird, *Senior Member, IEEE*, and Andrew M. Weiner, *Fellow, IEEE*

***Abstract*—We report the first quantitative study of intensity noise induced in line-by-line pulse shaping in response to time-varying changes in the comb frequency offset. Controllable comb linewidth broadening is synthesized through frequency dithering of a continuous-wave laser that is fed to a phase modulator. An electrical spectrum analyzer is used to examine the current power spectra of shaped time-domain intensity waveforms subject to comb frequency noise. A theoretical model predicting a 20 dB/decade scaling relation between the dither-induced noise and the frequency dither amplitude is presented. A numerical simulation method capable of predicting the precise form of the RF power spectrum in the presence of optical frequency dithering is explained. Two line-by-line shaping cases are considered in detail. Experimental data are in excellent agreement with the simulated results down to frequency dithers of a few tenths of a percent of the comb spacing. Tolerances to laser frequency fluctuations are given for several simple pulse shaping examples. The effect of pulse shaper parameters is also discussed.**

***Index Terms*—Optical arbitrary waveform generation, optical frequency comb, optical pulse shaping, signal analysis.**

I. Introduction

FOURIER transform optical pulse shaping is a well-established technique, in which user-defined time-domain waveforms are generated via manipulation in the spectral domain [1]. Recently, we have demonstrated line-by-line pulse shaping, in which the intensity and phase of each spectral line of an input pulse train (frequency comb) are independently controlled [2], [3]. In line-by-line shaping, the spectral resolution of a shaper is made finer than the repetition frequency, leading to shaped waveforms extending throughout the full time period between initial input pulses. Compared to previous pulse shaping works in which spectral lines were addressed only in groups, this constitutes an important step toward true optical arbitrary waveform generation.

As a consequence of line-by-line shaping, waveform contributions from overlapping adjacent pulses interfere coherently, resulting in a new source of time-domain waveform noise sensitive to variations in the comb offset frequency [2]. Thus, characterization of waveform intensity noise induced by fluctuations of the laser frequency (effective linewidth) and understanding of the resulting requirements for the frequency stability of the laser source become important issues in line-by-line pulse shaping. Different laser systems exhibit different ranges of frequency fluctuations. For example, mode-locked lasers generating combs of frequencies stabilized down to subhertz linewidths have resulted in revolutionary advances in optical frequency metrology [4] and optical carrier envelope phase control [5], [6]. However, these self-referenced mode-locked lasers typically operate at repetitions rates of $\sim$1 GHz and below, with line spacing too narrow for most pulse shapers to cleanly resolve. Frequency combs from high repetition rate sources such as harmonically mode-locked fiber lasers often suffer from supermode noise leading to frequency instabilities on the many hundred megahertz or even gigahertz scale, which lead to serious pulse shaping noise in line-by-line pulse shaping [2]. Some examples of frequency-stabilized ($\sim$megahertz linewidth) high repetition rate mode-locked fiber lasers and external-cavity semiconductor lasers have been demonstrated, but only with complicated control and/or compromised frequency tuning ability [7], [8]. Monolithic semiconductor mode-locked lasers are capable of generating high-repetition-rate pulses, with linewidths ranging from a few kilohertz to a few megahertz, increasing for higher repetition rates and often suffering from frequency chirps [9]. Frequency combs generated via phase modulation of a continuous-wave (CW) laser [10]–[12] have also been employed in line-by-line pulse shaping experiments [3], [13]–[17]. Such phase-modulated (PM) CW (PMCW) combs have an offset frequency determined by a CW laser, with a linewidth (of order 10 kHz in our experiments) intermediate between that of self-referenced mode-locked lasers and harmonically mode-locked lasers.

In a previous report, we performed a quantitative investigation of waveform changes in line-by-line pulse shaping induced due to *static* shifts of the optical comb frequency offset [18]. This work exploited the fact that with a PMCW comb, the frequency offset of individual lines is controlled by the input CW

Manuscript received March 12, 2008; revised May 30, 2008 and July 10, 2008. Current version published May 15, 2009. This work was supported by the Defense Advanced Research Project Agency/Air Force Office of Scientific Research under Grant FA9550-06-1-0189 and in part by the National Science Foundation under Grant ECCS-0601692.

C.-B. Huang is with the Institute of Photonics Technologies, National Tsing Hua University, Hsinchu, Taiwan (e-mail: robin@ee.nthu.edu.tw).

Z. Jiang is with the Beckman Institute, University of Illinois at Urbana-Champaign, Urbana-Champaign, IL 61801 USA (e-mail: zjiang@uiuc.edu).

D. E. Leaird and A. M. Weiner are with the School of Electrical and Computer Engineering, Purdue University, West Lafayette, IN 47907 USA (e-mail: leaird@purdue.edu; amw@purdue.edu).

Color versions of one or more of the figures in this paper are available online at http://ieeexplore.ieee.org.

Digital Object Identifier 10.1109/JQE.2009.2013148

0018-9197/$25.00 © 2009 IEEE

Authorized licensed use limited to: Purdue University. Downloaded on October 15, 2009 at 10:49 from IEEE Xplore. Restrictions apply.

laser and decoupled from the pulse generation process. This provides a degree of control not yet readily available from most high repetition rate (e.g., 2.5–10 GHz) mode-locked sources [7], [8]. By shifting the CW laser center frequency, the frequencies of all the comb lines are shifted accordingly, while leaving the relative powers, spacing, and phases of the lines unchanged. Relatively large static frequency offsets (up to 50%) were intentionally introduced in [18], so the impact on the generated time-domain waveforms could be clearly observed using a sampling oscilloscope. Our results showed that the amplitude of waveform changes due to optical frequency shifts at the input to a line-by-line shaper depends on the temporal position within the output waveform.

In practical laser systems, however, frequency fluctuations are time-dependent and occur with different amplitudes. In the current paper, we report a quantitative study of intensity noise induced in line-by-line pulse shaping in response to *time-varying* or *dynamic* changes in the comb frequency offset. In particular, we dither the comb offset frequency to controllably broaden the bandwidths of comb lines to values between 0.1% and 10% of the comb spacing. In this scheme, the frequency variations of different comb lines are completely correlated. This situation is relevant for lasers that are locked in repetition rate but not in offset frequency, such as most harmonically mode-locked lasers. The effect of such dynamic optical frequency shifts is characterized by measuring the resulting RF spectra via an electrical spectrum analyzer (ESA), which gives improved sensitivity as compared to the sampling oscilloscope measurements of [18].

It is worth noting that for the case of mode-locked lasers limited by quantum noise sources, the pulse timing and the overall phase (as opposed to the offset frequency) are considered to be the fundamental pulse parameters that fluctuate in response to noise [19], [20]. Due to the pulse timing fluctuations, which change the comb spacing, the comb lines at the edges of the spectrum are expected to exhibit greater frequency fluctuations than those near the carrier frequency. Although such effects are not considered in the current study, in principle, it should be possible to simulate fluctuations in the comb spacing by introducing modulation or fluctuations into the RF frequency driving the phase modulator of our PMCW source.

We have developed a theoretical model and a computational methodology that reliably and quantitatively predict the observed RF spectra as a function of synthesized optical linewidth; and we test our model by comparing with two experimental examples of line-by-line pulse shaping. Our current study provides a linkage between the variance of the comb offset frequency and the resulting variance introduced in the time-domain waveforms after line-by-line pulse shaping. From our results, the tolerance of line-by-line shaping to laser linewidth can be determined for different cases of pulse shaping. We note that although pulse shaping usually provides a large number of degrees of freedom, here we consider very simple shaped waveforms. This is similar to our philosophy in [15], where consideration of simple shaped waveforms provided insight into requirements for spectral resolution and power extinction ratio in line-by-line pulse shaping (but without consideration of fluctuations). The intent here is to use simple shaped waveforms

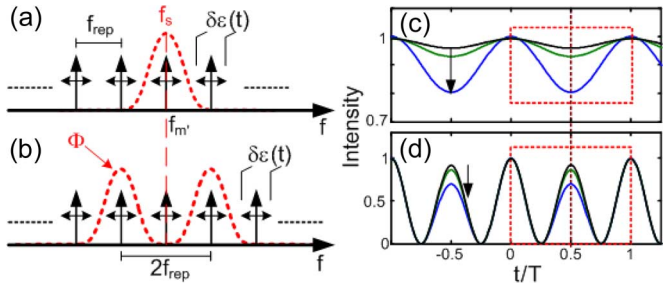

Fig. 1. Schematic of comb line filtering from an optical frequency comb with line spacing of $f_{\rm rep}$ and time-varying comb offset variation $\delta\varepsilon(t)$. (a) Single-line filtering case. (b) Two-line filtering with spacing of $2\,f_{\rm rep}$. Effective shaper filter functions are shown as dotted traces. Filter center frequency f_s is denoted by the dashed line. Corresponding time-domain intensities for (c) single-line and (d) two-line with $\Phi = 0$ filtering cases under static comb offsets of {0%, 10%, and 20%} are shown using the method reported in [18]. In (c) and (d), the arrows indicate the waveform evolutions with increasing offsets. The dashed squares denote waveforms for one period $T = 1/f_{\rm rep}$. Initial pulse locations are at integer multiples of *T*. The dotted line denotes temporal position of *T*/2. Maximum time-domain intensity variations happen at temporal position of *T*/2, as explained using the time-domain point of view in [2].

to develop waveform fidelity metrics relevant to time-dependent optical frequency fluctuations. The machinery that we develop may also be applied to specific cases of complex pulse shaping as desired.

The remainder of this paper is organized as follows. In Section II, we discuss two very simple line-by-line pulse shaping examples that will be studied in our frequency dithering experiments. In Section III, we describe our experimental setup and measurement system limitations. Section IV presents a simple theoretical model for the RF power spectrum induced by optical frequency fluctuations and describes a numerical method whereby RF spectra may be computed quantitatively. In Section V, experimental RF spectra are presented and compared to the calculations. In Section VI, we discuss simulation results that provide insight into the effect of pulse shaper parameters such as spectral resolution. Section VII ends with the conclusion.

II. Test Waveforms

Two simple line-by-line pulse shaping operations sensitive to the frequency comb offsets are illustrated in Fig. 1 [15], [18]. Fig. 1(a) schematically depicts filtering of a single line from an optical frequency comb with lines spaced by repetition frequency $f_{\rm rep}$, while Fig. 1(b) depicts selection of two lines with one intermediate line blocked and with an adjustable relative phase Φ applied to one of the selected lines. The frequency positions of the comb lines can be expressed as [5]

$$f_m = m f_{\rm rep} + \varepsilon + \delta\varepsilon(t) \tag{1}$$

where m are large integers, ε denotes a static comb frequency offset, and $\delta\varepsilon(t)$ is an additional time-varying offset frequency introduced in our experiments. As explained in [18], only the relative frequency offset relative to the features of the pulse shaping mask will be important for this investigation. In Fig. 1(a) and (b), the corresponding shaper filter functions are shown as dotted traces. The center frequency $f_{\rm s}$ (dashed line) of the filter function serves as a frequency reference.

Authorized licensed use limited to: Purdue University. Downloaded on October 15, 2009 at 10:49 from IEEE Xplore. Restrictions apply.

Fig. 1(c) and (d) shows the calculated time-domain intensity waveforms for single-line and two-line filtering ($\Phi = 0$) cases, respectively, with static comb offsets of {0%–20%} in 10% per increment. The calculation method will be described in Section III and is also reported in detail within [18].

For single-line filtering shown in Fig. 1(a) and (c), the waveforms evolve from a constant intensity CW signal to a strongly modulated waveform under comb frequency offset. For the two-line filtering at $2f_{\rm rep}$ case shown in Fig. 1(b) and (d), the waveform initially consists of two equal intensity peaks per $f_{\rm rep}$ period (it is periodic at 2 $f_{\rm rep}$), but under increasing frequency offset one of the two pulses per period loses intensity. The phase of one of the lines can be shifted by a controllable amount Φ to allow further investigations on noise contributed through pulse shaping. In both cases, the waveforms vary most strongly at temporal positions where adjacent input pulses provide equal contributions, and hence, interference most effectively. This occurs exactly between the original pulses (at $\pm T/2$), consistent with previous experimental observations [2]. Note that ideally both optical intensity waveforms selected for study should have no corresponding $f_{\rm rep}$ frequency component in their RF spectra when the frequency offset is zero. Hence, one may expect the RF spectra in the vicinity of $f_{\rm rep}$ to respond sensitively to either static frequency offsets or a time-varying frequency dither introduced in our experiments. In practice, both finite extinction ratio and finite spectral resolution in the pulse shaper lead to a finite amplitude for the $f_{\rm rep}$ harmonic in the RF spectrum even without frequency offset or dither. Nevertheless, investigation of these simple waveforms will provide new and quantitative insight into time-dependent pulse shaping noise introduced through fluctuations of the comb offset frequency.

III. Experimental Setup

Fig. 2(a) shows the schematic experimental setup. A 1-kHz-linewidth CW laser (Koheras Adjustik) with intra-cavity piezoelectric transducer (PZT) is phase-modulated by a lithium niobate phase modulator (PM: 12.5 GHz bandwidth, $V_\pi \sim 5$ V at 10 GHz) driven at repetition frequency $f_{\rm rep} = 9.15$ GHz (~ 0.91 V_π peak to peak) by the clock signal from a bit-error-rate test (BERT: Agilent N4901B). The driving frequency is set to precisely map the spectral line spacing of the resultant frequency comb to the pixel spacing of the pulse shaper. A sinusoidal signal is used to provide controllable comb linewidth broadening $\delta\varepsilon(t)$ with dithering frequency $f_{\rm d} = 10$ kHz. The resulting PMCW comb is sent to a reflective 9.15-GHz line-by-line shaper, similar to that described in detail within [15]. Discrete comb lines are diffracted by the grating and focused by a lens with 1000 mm focal length. A 2×128 pixel liquid crystal modulator (LCM) array is placed just before the lens focal plane to independently control both amplitude and phase of individual spectral lines. A mirror is placed at the minimum focusing plane, leading to double-pass geometry, with all the spectral lines recombined into a single fiber and separated from the input via an optical circulator. Amplitude manipulation is realized by LCM control and the polarization extinction of the polarization beam splitter (PBS) in the recombination path back into the collimator.

For a grating-based free-space pulse shaper, the effective frequency-domain filter function $H(\omega)$ that characterizes its response as a linear filter can be obtained by convolving the programmable spatial masking function $M(x)$ defined by the LCM with the Gaussian intensity profile of a single optical frequency beam

$$H(\omega) = \left(\frac{2}{\pi w_0^2}\right)^{\frac{1}{2}} \int M(x) e^{\frac{-2(x-\alpha\omega)^2}{w_0^2}} dx \qquad (2)$$

where w_0 is the Gaussian beam radius (half-width at $1/e_2$ of intensity) and α is the spatial dispersion with units centimeter per radian per hertz [1]. In the experiment, the frequency lines have a 9.15 GHz spacing, with each line having a Gaussian spatial profile of radius $w_0 = 95$ μm. Each LCM pixel has a 100 μm width and a corresponding frequency span of 4.575 GHz; therefore, frequency lines are centered on every second LCM pixel (using two LCM pixels to control each line). Our line-by-line shaper has $\alpha = 3.60^{*}10^{-13}$ cm $(\text{rad/s})^{-1}$ and a full-width at half-maximum spectral resolution of 2.6 GHz. Such resolution ensures observation of temporal overlapping contributions from adjacent pulses. After pulse shaping, optical intensity is converted to photocurrent by a 20 GHz photodetector and measured using a 50-GHz bandwidth sampling scope and an electrical spectral analyzer.

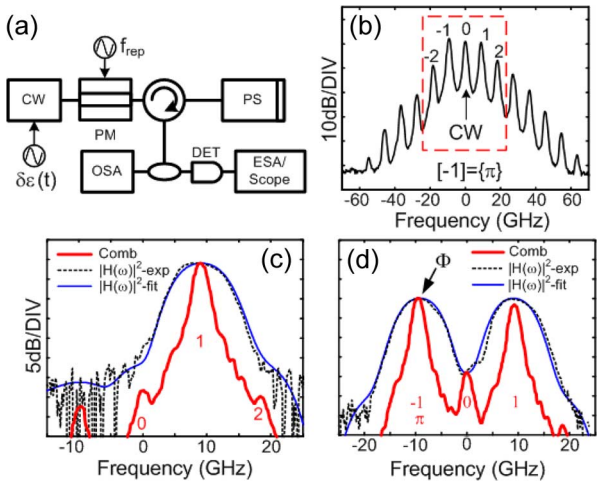

Fig. 2. (a) Experimental setup using a PMCW laser frequency comb with repetition frequency of $f_{\rm rep}$. PM: phase modulator; $\delta\epsilon(t)$: controllable comb linewidth broadening; PS: pulse shaper; OSA: optical spectrum analyzer; Scope: 50-GHz bandwidth sampling scope. (b) Optical spectrum of the PMCW comb. Line numbered {0} denotes the CW laser frequency. Line {−1} is intrinsically π out of phase. (c) Single-line filtering after the shaper. (d) Two-line filtering with spacing $2f_{\rm rep}$ after the shaper. Line {−1} is applied with phase control Φ to examine shaping effects. $\Phi = 0$ for the figure shown. In (c) and (d), filtered comb lines are shown using bold traces; experimental (dotted) and fitted (solid) filter functions are plotted for both cases.

Fig. 2(b)–(d) shows optical spectra obtained without frequency dithering using an optical spectrum analyzer (OSA: Ando 6317B) with 0.01 nm resolution. Fig. 2(b) shows the resulting PMCW comb spectrum without any intensity/phase control from the shaper. The comb lines used in this paper are highlighted by the dashed square and numbered from −2 through 2. Comb line frequencies are defined relative to the CW laser frequency, marked by the arrow. All the lines between {−2 and 2} are in phase, except for line {−1}, which is shifted by π, as measured using the method reported in [21]. Filtered comb lines are shown using bold traces in Fig. 2(c) and (d).

Authorized licensed use limited to: Purdue University. Downloaded on October 15, 2009 at 10:49 from IEEE Xplore. Restrictions apply.

$|H(\omega)|^2$ (dotted traces) are experimentally acquired using an amplified spontaneous emission source as input to the shaper. Fitted $|H(\omega)|^2$ (solid traces) are also plotted for both cases. Fig. 2(c) shows the experimental spectrum of single-line filtering (only line {1} selected). Fig. 2(d) shows the two-line filtering at $2f_{\rm rep}$ case, where lines $\{-1\}$ and {1} are selected by the shaper and with line {0} suppressed. In Fig. 2(c) and (d), the small imperfectly suppressed lines are due to the finite power extinction ratio (~20 dB). In our experiments, two razor blades are used to block the deselected spectral portions from both ends for improved power extinction ratio (>30 dB). Finite power extinction ratio is governed by two main parameters: $w_0$and the polarization extinction ratio of the shaper. This is more apparent in Fig. 2(d), where the suppression of line {0} is limited by 20 dB. In fitting for experimental $|H(\omega)|^2$, finite extinction ratio is taken into account by giving a nonzero amplitude, for example, $M(x) = 0.1$ (−20 dB in power) for pixels controlling line {0}. Similarly, in simulating the slightly asymmetric experimental lineshape function in Fig. 2(c), we set $M(x)$ to small but different nonzero values on either side of selected line in order to best fit the experimental data. The effects of these unsuppressed peaks on our waveform measurements will be discussed in later sections.

The effective width broadening of the comb lines in our experiments is achieved by applying an amplified sinusoidal signal from a function generator at $f_{\rm d} = 10$ kHz dithering frequency to the PZT. We controllably broaden the comb lines through the relation

$$\delta\varepsilon(V,t) = A_d(V)\sin(2\pi f_d t) \tag{3}$$

where $A_{\rm d}$ is the maximum frequency dithering amplitude, V is the root-mean-square voltage of the applied sinusoidal signal in volts, controlled through varying the gain of a linear electrical amplifier. Measurement of the linewidth broadening is performed using a conventional heterodyne beating setup [22]. The dithered CW laser field is combined through an optical coupler with a second CW laser field (HP 81680A, linewidth of 16 MHz). Beat signals are detected using a 20-GHz-bandwidth photodetector (DET) and measured with an electrical spectrum analyzer (ESA: Agilent 8565EC with 30 Hz to 50 GHz) in maximum-hold function for 30 s. Fig. 3(a) shows the heterodyne beating results for 6 and 30 V (rms) applied to the PZT of CW1, resulting in total linewidth broadening $(2A_{\rm d})$ of 0.21 and 1.08 GHz, respectively. The $A_{\rm d}(V)$ relation determined from the heterodyne beatings with CW2 is plotted in Fig. 3(b). The heterodyne results show a linear response; the effective comb linewidth broadening is determined through

$$A_{\rm d}(V) = 0.018\ {\rm V} \tag{4}$$

where the units of $A_{\rm d}$ and V are gigahertz and (rms) volts, respectively. Thus, by frequency dithering laser CW1 and then feeding it into the PM setup, we are capable of controllably and simultaneously broadening all the comb lines for a PMCW comb.

As an example of time-dependent intensity noise introduced through frequency fluctuations (dither), Fig. 4 shows data acquired using the fast oscilloscope. In this example, two-line

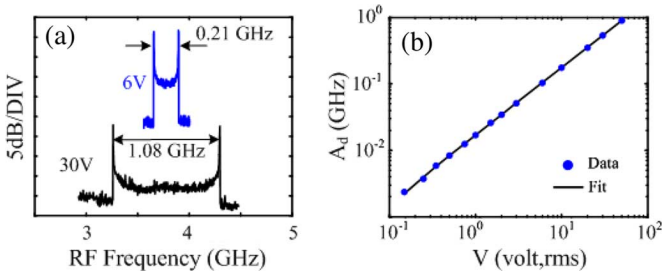

Fig. 3. (a) Heterodyne beating results for 6 and 30 V (rms) applied to the PZT. (b) Relation between frequency dithering amplitudes $(A_{\rm d})$ and applied rms voltage (V) to the PZT.

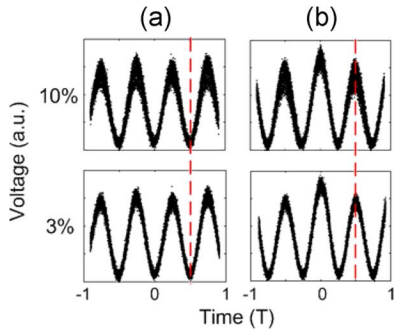

Fig. 4. 50 overlaid sampling scope traces with dithering amplitude of 10 and 3% (compared to the 9.15 GHz comb spacing) for two-line filtering with phase control $\Phi = \{0({\rm a})\ {\rm and}\ \pi({\rm b})\}$ applied to line $\{-1\}$ shown in Fig. 3(d). T/2 positions are marked using the dashed lines.

filtering (lines $\{-1, 1\}$ selected) is applied with a phase shift of either $\Phi = 0$ or $\Phi = \pi$ applied to line $\{-1\}$. The figure consists of 50 overlaid sampling scope traces with frequency dither amplitudes of either 10% or 3%, relative to the 9.15-GHz comb spacing. Temporal delays are referenced to the cosine waveform peaks obtained by first selecting only lines {0, 1}. Ripple in the intensity of different peaks is caused by imperfect suppression of deselected lines. Note that line $\{-1\}$ as generated via the phase modulation already has a π phase shift. Thus, programming the LCM $\Phi = \pi$, as in Fig. 4(b), corrects the phase and brings the waveform peaks to zero delay. Fig. 4(b) with 10% dither amplitude clearly illustrates our expectation that larger intensity noise is observed at $T/2$ (marked by the dashed lines) than at zero-time position. As for Fig. 4(a), since all peaks are equally spaced from $T/2$ and zero, they have the same noise amplitude. Time-domain intensity noise clearly decreases when the dithering amplitude is reduced. However, reduction in noise amplitude is difficult to assess from the scope traces for dithering amplitudes less than 6%. Therefore, for more sensitive characterization of waveform noise induced through frequency dithering, in the rest of the paper, we use an ESA as our preferred diagnostic tool.

To be capable of distinguishing the optical frequency modulation to amplitude modulation (FM–AM) noise induced through pulse shaping, one needs to know whether the laser itself generates FM–AM noise. Therefore, we calibrate our measurement system and provide direct comparisons using the following two setups without the phase modulator: in configuration 1, the CW laser is measured directly on an ESA after the photodetector

Authorized licensed use limited to: Purdue University. Downloaded on October 15, 2009 at 10:49 from IEEE Xplore. Restrictions apply.

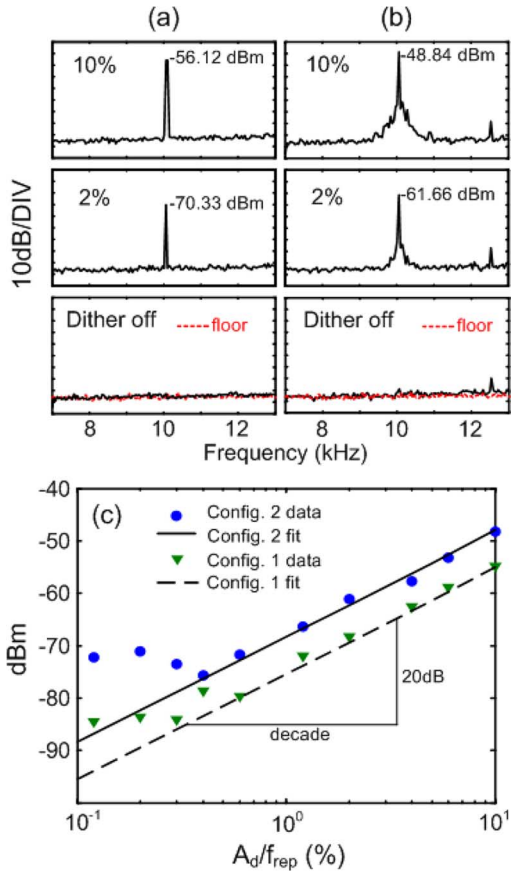

Fig. 5. ESA measurements centered at $f_{\rm d} = 10$ kHz with dithering amplitude $A_{\rm d}/f_{\rm rep} = \{10\%,\ 2\%$ and $0\%\}$, compared to the 9.15-GHz comb spacing, for configurations 1 (a) and 2 (b). System noise floor (dotted trace) is determined with no optical input power to the photodetector. In both figures, the traces are obtained by maximum holding the ESA for 5 min with resolution bandwidth of 3 Hz. Noise peak values are indicated. (c) Noise peak values for configuration 1 (triangle) and 2 (dot) and fitting curves against dither amplitudes are plotted. Data fitting reveals a 20 dB/decade scaling relation.

with variable optical attenuator in between; while in configuration 2, the CW laser is sent to the shaper with single-line filter as shown in Fig. 2(c) and measured. Optical power into the photodetector is 3.5 dBm in both configurations.

Fig. 5 shows the ESA measurements centered at dithering frequency $f_{\rm d} = 10$ kHz. Fig. 5(a) and (b) shows ESA traces with a dithering amplitude $A_{\rm d}/f_{\rm rep} = \{10\%,\ 2\%,$ and $0\%\}$, relative to the 9.15-GHz comb spacing, for configurations 1 and 2, respectively. The system noise floor, determined with no input power into the photodetector, is also plotted within the dithering-off figures. As expected, the laser intrinsically generates FM–AM noise peaks [Fig. 5(a)]. However, in both figures, noise peaks at $f_{\rm d}$ are evidently higher for configuration 2, revealing extra noise attributed to pulse shaping effects. For closer examinations, Fig. 5(c) shows the noise peak values for configuration 1 (triangle) and configuration 2 (dot) along with linear fitting curves for various dither amplitudes. Here, we note two observations: 1) for dithering amplitudes of $\{0.4\%$–$10\%\}$, configuration 2 gives a roughly 7.5 dB extra noise peak for all dithering amplitudes and 2) the wings of the peaks for configuration 2 show a broadening that is not observed in configuration 1. To test the origin of these observations, we programmed the shaper for unity transmission for all pixels (no filtering). We observed that the amplitudes of the noise peaks reduced to the same values as configuration 1. This confirms that the increased amplitude in the noise peaks is a filtering effect. We also observed that the broadening of the wings remains even when the pulse shaper is programmed for unity transmission for all pixels. Therefore, we attribute the broadened wings to low-frequency mechanical vibrations that affect free space to fiber coupling within our fiber-coupled pulse shaper. Data fitting in Fig. 5(c) reveals a 20 dB/decade relation, which will be explored in the following sections. For dithering amplitudes smaller than 0.4%, noise peaks depart from the fitting curve in both configurations. This may indicate residual amplitude noise arising from modulation of the PZT that persists even at low dither amplitudes.

IV. Theoretical Model and Numerical Method

A. Theoretical Model

Here, we present a theoretical derivation to characterize comb frequency dither-induced noise of line-by-line shaped waveforms using an ESA. In the spirit of [23], we first define the waveform intensity as

$$P(t) = P_0(t) + P_\nu(t)\nu(t) + \delta P(t) \tag{5}$$

where $P_0(t)$ denotes the ideal, fluctuation-free pulse train, $P_\nu(t)$ denotes the first derivative of the waveform after the line-by-line shaper with respect to frequency fluctuation $\nu(t)$, and $\delta P(t)$ denotes waveform variations due to other noise mechanisms. Here we first note that both $P_0(t)$ and $P_\nu(t)$ are periodic waveforms with a same periodicity of $T = 1/f_{\rm rep}$.

When waveform variations due to amplitude and timing jitters are also taken into account, we can express the waveform as

$$P(t) = [1 + A(t)]\left[P_0\left(t - \delta T(t)\right) + P_\nu\left(t - \delta T(t)\right)\nu(t)\right] \tag{6}$$

where $A(t)$ and $\delta T(t)$ denote the amplitude and timing jitter terms, respectively. The output detector current is obtained by convolving the waveform intensity with the impulse response function $g_{\rm PD}(t)$ of the photodetector

$$I_{\rm PD}(t) = g_{\rm PD}(t) \otimes P(t). \tag{7}$$

Under the assumption of a small timing jitter and when $A(t)$, $\delta T(t)$, and $\nu(t)$ are uncorrelated zero-mean functions, we can express the power correlation function of the optical waveform as

$$\begin{aligned}
&\langle P(t)P(t-\tau)\rangle \\
&\quad = [1 + \langle A(t)A(t-\tau)\rangle] \\
&\qquad \cdot [\langle P_0(t)P_0(t-\tau)\rangle + \langle P_\nu(t)P_\nu(t-\tau)\rangle \langle \nu(t)\nu(t-\tau)\rangle \\
&\qquad\quad + \left\langle \dot{P}_0(t)\dot{P}_0(t-\tau)\right\rangle \langle \delta T(t)\delta T(t-\tau)\rangle \\
&\qquad\quad + \left\langle \dot{P}_\nu(t)\dot{P}_\nu(t-\tau)\right\rangle \langle \nu(t)\nu(t-\tau)\rangle \\
&\qquad\quad \times \langle \delta T(t)\delta T(t-\tau)\rangle]
\end{aligned} \tag{8}$$

where the $(\dot{\bullet})$ represents the derivative with respect to time.

Authorized licensed use limited to: Purdue University. Downloaded on October 15, 2009 at 10:49 from IEEE Xplore. Restrictions apply.

The current power spectrum with frequency dithering measured on an ESA is therefore expressed as [23]

$$\left|\widetilde{I}(\omega)\right|^2 = \left|\widetilde{G}_{PD}(\omega)\right|^2 \cdot \left[\delta(\omega) + \left|\widetilde{A}(\omega)\right|^2\right] \otimes \left[\left|\widetilde{P}_0(\omega)\right|^2 + \left|\widetilde{P}_\nu(\omega)\right|^2 \otimes |\widetilde{\nu}(\omega)|^2\right] \otimes \left[\delta(\omega) + \omega^2 \left|\delta\widetilde{T}(\omega)\right|^2\right]. \quad (9)$$

Here $\otimes$ denotes convolution. $\widetilde{G}_{\mathrm{PD}}(\omega)$, $\widetilde{P}_0(\omega)$, $\widetilde{P}_\nu(\omega)$, $\widetilde{\nu}(\omega)$, and $\delta\widetilde{T}(\omega)$ denote the baseband frequency response of $G_{\mathrm{PD}}(t)$, $P_0(t)$, $P_\nu(t)$, $\nu(t)$, and $\delta T(t)$ obtained through the Fourier transform relation, respectively.

Disregarding the term with the products of $|\widetilde{A}(\omega)|^2$ and $|\delta T(\omega)|^2$, we obtain

$$\left|\widetilde{I}(\omega)\right|^2 = \left|\widetilde{G}_{\mathrm{PD}}(\omega)\right|^2 \cdot \left\{\left|\widetilde{P}_0(\omega)\right|^2 + \left|\widetilde{P}_\nu(\omega)\right|^2 \otimes |\widetilde{\nu}(\omega)|^2\right\} \otimes \left\{\delta(\omega) + \left|\widetilde{A}(\omega)\right|^2 + \omega^2 \left|\delta\widetilde{T}(\omega)\right|^2\right\}. \quad (10)$$

At this point we provide several comments related to (10):

1) Both $|\widetilde{P}_0(\omega)|^2$ and $|\widetilde{P}_\nu(\omega)|^2$ consist of a sequence of RF harmonics at frequencies $\omega_k = k(2\pi f_{\mathrm{rep}})$.
2) The frequency dithering terms grow as $|\widetilde{\nu}(\omega)|^2$, and thus, follows a 20 dB/decade scaling relation with respect to the amplitude of the frequency dithering function.
3) Our analysis applies to a general dithering function $\nu(\mathrm{t})$. However, in our experiment, the frequency dithering is applied using a time-domain sinusoidal function (frequency f_{d}), and thus, $|\widetilde{\nu}(\omega)|^2$ consists of delta functions at $\omega = \pm 2\pi \mathrm{f_d}$. Hence, the frequency dithering introduces new peaks into the measured ESA spectrum at $\pm f_{\mathrm{d}}$ with respect to the harmonics at kf_{rep}.
4) We can thus quantify the waveform fluctuation due to frequency offset variation by introducing the normalized variance as

$$\frac{\left\langle [P_\nu(t)\nu(t)]^2 \right\rangle}{\langle P_0^2(t)\rangle} = \frac{\int \left|\widetilde{P}_\nu(\omega) \otimes \widetilde{\nu}(\omega)\right|^2 d\omega}{\int \left|\widetilde{P}_0(\omega)\right|^2 d\omega}. \quad (11)$$

Assuming negligible (or separable) amplitude and timing jitter, the normalized variance can be obtained through the photocurrent power spectrum by the following notation

$$\frac{\left\langle [P_\nu(t)\nu(t)]^2 \right\rangle}{\langle P_0^2(t)\rangle} = \frac{\sum_k \left[\int_{\omega_k - \delta\omega_{\min}}^{\omega_k - \delta\omega_{\max}} + \int_{\omega_k + \delta\omega_{\max}}^{\omega_k + \delta\omega_{\min}}\right] \left|\widetilde{I}(\omega)\right|^2 d\omega}{\sum_k \int_{\omega_k - \Delta\omega_{\mathrm{RB}}}^{\omega_k + \Delta\omega_{\mathrm{RB}}} \left|\widetilde{I}(\omega)\right|^2 d\omega} = \frac{\sum_k E_{\mathrm{noise},k}}{\sum_k E_{0,k}}. \quad (12)$$

Here, the powers of the unperturbed harmonic peaks $(E_{0,k})$ are integrated over the ESA resolution bandwidth $(\Delta\omega_{\mathrm{RB}})$ for each harmonic, while the contributions to the noise power $(E_{\mathrm{noise},k})$ are integrated over a specified frequency range between $\delta\omega_{\min}$ and $\delta\omega_{\max}$ for all harmonics. Evidently, one would require $\delta\omega_{\min} \geq \Delta\omega_{\mathrm{RB}}$; the value of $\delta\omega_{\max}$ will depend on the highest frequency content of the dithering signal, but is evidently less than $\pi \mathrm{f_{rep}}$. Since the waveform may change in a complicated way with offset frequency variation, we may obtain more information by looking at contributions to normalized variance from a particular harmonic (single k value at a time). In this manner, we may obtain an estimate of the quantity

$$\eta_{k,p} \equiv \frac{E_{\mathrm{noise},k}}{E_{0,p} \cdot \int |\widetilde{\nu}(\omega)|^2 d\omega}. \quad (13)$$

The frequency-dither-induced noise associated with the kth harmonic $(E_{\mathrm{noise},k})$ is normalized to a desired pth (where $p \geq 1$) harmonic peak of the unperturbed signal $(E_{0,p})$ and the variance of the offset frequency fluctuation. Thus, the factor $\eta_{k,p}$ (with unit of decibels relative to the carrier per hertz) gives the proportionality constant linking the output intensity waveform variation of the kth RF harmonic to the variance of the offset frequency, normalized to the pth RF harmonic of the shaped intensity waveform without frequency noise. This constant is actually independent of the form of the power spectral density of the frequency offset fluctuations, but does depend on harmonic number and the line-by-line shaper filter function. In the following sections, we compute this constant for the special case of a sinusoidal frequency offset dithering and confirm our computations by experiments.

5) From (10), it is noted that both the harmonics of the unperturbed waveform as well as those associated with waveform derivatives with respect to frequency-offset fluctuations are affected by amplitude and timing jitters in a similar way. For our special case of a single-tone dithering signal, the harmonics at kf_{rep} and the dither terms arising at $kf_{\mathrm{rep}} \pm \mathrm{f_d}$ have the same line shape, as will be presented in Section V.
6) Higher order terms not included in the current analysis can lead to additional noise peaks in the RF spectrum, e.g., at frequencies $kf_{\mathrm{rep}} \pm 2f_{\mathrm{d}}$, which follow a 40 dB/decade scaling relation with respect to frequency dithering amplitude and so forth.

B. Numerical Method

Here, we explain our numerical method for calculating the ESA current power spectrum under frequency dithering. The flow of the method is outlined in Fig. 6(a). Our numerical approach is capable of obtaining the higher order terms described in the previous section. First, we define two time variables: a fast time variable t (with its corresponding fast frequency denoted as ω) on the scale of pulse repetition, and a slow time variable t' (with its corresponding slow frequency denoted as ω') on the time scale of frequency dithering. Next, frequency

Authorized licensed use limited to: Purdue University. Downloaded on October 15, 2009 at 10:49 from IEEE Xplore. Restrictions apply.

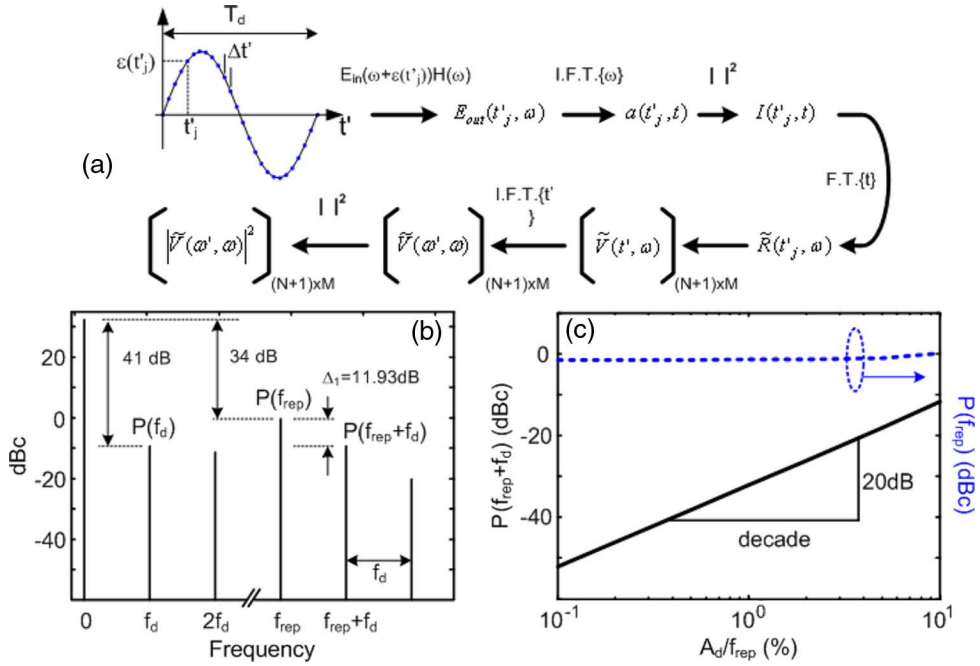

Fig. 6. (a) Flow chart of the numerical method. (b) Calculated current power spectrum for the single-line filtering case with 10% dithering amplitude, showing beats from dc to $2f_{\rm d}$ and $f_{\rm rep}$ to $f_{\rm rep}+2f_{\rm d}$. Noise peak values at $f_{\rm d}$, $f_{\rm rep}$, and $f_{\rm rep}+f_{\rm d}$ are labeled $P(f_d)$, $P(f_{\rm rep})$, and $P(f_{\rm rep}+f_{\rm d})$, respectively. Δ_1 denotes the power ratio between $P(f_{\rm rep})$ and $P(f_{\rm rep}+f_{\rm d})$. (c) Simulated relationship of $P(f_{\rm rep}+f_{\rm d})$ and $P(f_{\rm rep})$ to various dithering amplitudes.

variations within one dithering period ($T_{\rm d}=1/f_{\rm d}$) are numerically sampled using $N+1$ evenly spaced temporal points with time interval given by $\Delta t'=T_{\rm d}/N$

$$\varepsilon\left(t'_j\right)\equiv A_d\sin\left(2\pi f_d t'_j\right),\quad j=1,2,\ldots,N+1 \tag{14}$$

where $\varepsilon(t'_j)$ denotes the *j*th static comb frequency offset value at time $t'_j=(j-1)\Delta t'$.

Using the comb line amplitudes and filter functions obtained through fittings in Fig. 2(b), corresponding output fields $E_{\rm out}(t'_j,\omega)$ for the *j*th sampling point are derived through the relation [18]

$$E_{\rm out}\left(t'_j,\omega\right)=E_{\rm in}\left(\omega+\varepsilon\left(t'_j\right)\right)\cdot H(\omega). \tag{15}$$

The corresponding output time-domain envelope function is obtained by inverse Fourier-transforming the output field with respect to the fast frequency scale ω

$$a\left(t'_j,t\right)=\frac{1}{2\pi}\int E_{\rm out}\left(t'_j,\omega\right)e^{j\omega t}d\omega. \tag{16}$$

Waveform intensities are obtained by equating $I(t'_j,t)=|a(t'_j,t)|^2$. The intensities are similar to what are shown in Fig. 1(c) and (d) for each static frequency offset value $\varepsilon(t'_j)$. For each $I(t'_j,t)$, the Fourier-series coefficients are calculated (for the fast frequency scale) using the waveform within one period ($T=1/f_{\rm rep}$, as shown within the dashed rectangle in Fig. 1(c)and (d)) to obtain the complex RF amplitude spectrum $\widetilde{R}(t'_j,\omega)$.

From $\widetilde{R}(t'_j,\omega)$, the complex amplitudes of each RF spectral component of interest are extracted and stored in a $(N+1)\times M$ matrix $\widetilde{V}(t',\omega)$, in such a way that the first column of $\widetilde{V}(t',\omega)$ records the dc values, the second column corresponds to $f_{\rm rep}$, the third column corresponds to $2f_{\rm rep}$ and so forth. In this critical step, we physically separate the two time scales, so that the $N+1$ values of each column of $\widetilde{V}(t',\omega)$ thus represent the time-domain evolution of the complex amplitude of the *m*th harmonic of $f_{\rm rep}$ within one dithering cycle, in the slow dithering time scale t'. Now, by performing a Fourier transform on $\widetilde{V}(t',\omega)$ with respect to t' and taking the absolute value squared, we arrive at the final current power spectrum array $|\widetilde{V}(\omega',\omega)|^2$

$$\left|\widetilde{V}(\omega',\omega)\right|^2=\left|\int\widetilde{V}(t',\omega)e^{-j\omega' t'}dt'\right|^2. \tag{17}$$

Along the *m*th column, the *j*th value denotes the noise peak of the ESA current power spectrum separated by $j(f_{\rm d})$ from $m(f_{\rm rep})$. In order to obtain accurate results, *N* should be made large enough so that $I(t'_j,t)$ and $I(t'_{j+1},t)$ do not change abruptly from one to the next. Comparison among results reveals that *N* greater than 100 is sufficient, making our method computationally efficient and tractable. Note that our numerical method is also applicable when multiple dithering tones are present simultaneously.

Resulting calculated beat signals from $\{{\rm dc}\sim 2f_{\rm d}\}$ and $\{f_{\rm rep}\sim f_{\rm rep}+2f_{\rm d}\}$ are shown in Fig. 6(b) for the single-line filtering case [experimental condition as shown in Fig. 2(c)] with a 10% sinusoidal dithering amplitude. Power peak values at frequencies of $\{f_{\rm d},f_{\rm rep},f_{{\rm rep}+f_{\rm d}}\}$ are denoted here as $\{P(f_d),P(f_{\rm rep}),P(f_{{\rm rep}+f_{\rm d}})\}$ and throughout the rest of the paper, respectively. The powers are normalized to $P(f_{\rm rep})$ [$p=1$ in (13)] and are in units of decibels relative to the carrier. For the ideal single-line filtering case with infinite shaper spectral resolution, the time-domain waveform should

Authorized licensed use limited to: Purdue University. Downloaded on October 15, 2009 at 10:49 from IEEE Xplore. Restrictions apply.

consist of a constant intensity waveform. In the current power spectrum, there should be no observable beat signals at $f_{\rm rep}$. However due to finite power extinction of the line-by-line shaper in practice, e.g., due to finite spectral resolution and imperfect polarization control by the LCM, one must take the unsuppressed intensity peaks into account, resulting in a 34 dB contrast between the dc and $f_{\rm rep}$ beat. By observation, the beat signal at $2f_{\rm d}$ is almost as large as $P(f_{\rm d})$. This is not surprising: in the ideal case, where comb line amplitudes and filter function are perfectly symmetric (even function) about the filter frequency center f_s, the first derivative term in (8) vanishes, resulting in peaks only at even multiples of $f_{\rm d}$. However, asymmetry caused by intrinsic variations in the line-to-line phase/amplitude of PMCW combs introduces the odd multiples of $f_{\rm d}$ experimentally. $\Delta_1 = 11.93$ dB denotes the power ratio between $P(f_{\rm rep})$ and $P(f_{\rm rep}+f_{\rm d})$ with a 10% dither amplitude. Fig. 6(c) shows the simulation results of $P(f_{\rm rep}+f_{\rm d})$ and $P(f_{\rm rep})$ against different dithering amplitudes, normalized to $P(\mathrm{f_{rep}})$ value with 10% dither amplitude. $P(f_{\rm rep})$ remains nearly constant. The prediction of a 20 dB/decade variation [discussion point 2) following (10)] in $P(f_{\rm rep}+f_{\rm d})$ from our theoretical model is confirmed. From this 20 dB/decade relation, we can find the factor $\eta_{1,1}$ for this shaping example by using the relation $\eta_{1,1} = -\Delta_1 - 20\cdot\log(915\ \mathrm{MHz})$ and obtain a value of -191.16(dBc/Hz).

These simulations are carried out using our current experimental pulse shaper parameters. We note here that specific values obtained for the dither-induced noise peaks will depend on the pulse shaper parameters, namely, LCM pixel spacing and the spectral resolution. If desired, our model can be applied to predict the effect of other pulse shaper settings by simply changing the masking function and spectral resolution as defined in (2). Some examples of shaper parameter effects are presented in Section VI.

V. Experimental Results and Discussions

A. Single-Line Filtering

We first examine the validity of our numerical model with only line {1} selected. Fig. 7 shows the results with dithering amplitude of 10%, and average optical power of -1.5 dBm into the photodetector. ESA measurements of $P(f_{\rm d})$, $P(f_{\rm rep})$, and $P(\mathrm{f_{rep}}+f_d)$ are shown in Fig. 7(a) and (b), respectively. Calculated noise peak values shown in Fig. 6(b) are normalized to experimental $P(f_{\rm rep})$ value. Experimental and calculated noise peak values are given within the figures and are in good agreement. Experimentally, a Δ_1 (ratio between $P(f_{\rm rep})$ and $P(f_{\rm rep}+f_{\rm d})$) value of 10.64 dB is obtained, in close agreement to the calculated value of 11.93 dB. The slight discrepancy can be attributed to the asymmetry of the experimental filter function.

Comparing Fig. 7(a) with (b), a clean spectrum is obtained in Fig. 7(a), while there are numerous extra noise peaks observed in Fig. 7(b). Fig. 7(c) shows maximum hold traces with 10% dithering amplitude, dithering turned off, and the system noise floor. The trace with dithering off reveals the extra noise pedestals are due to amplitude and timing jitter, which we attribute to the BERT driving the phase modulator. As derived

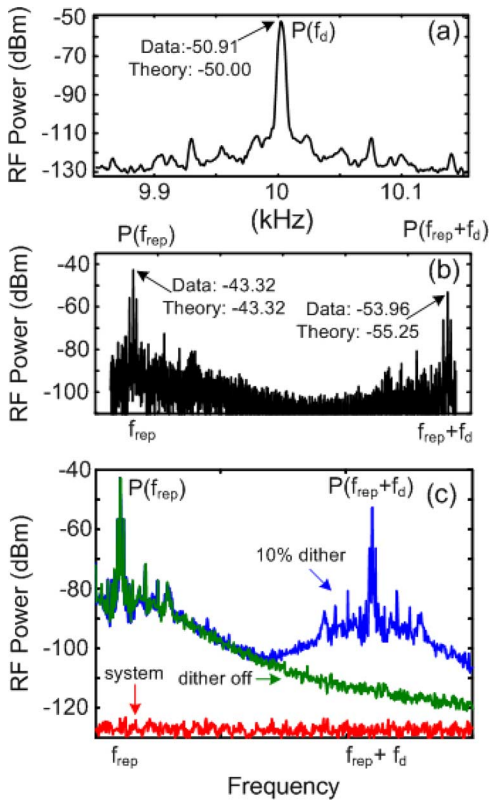

Fig. 7. Single-line filtering experimental results with $A_{\rm d}/f_{\rm rep} = 10\%$. (a) ESA measurement of $P(f_{\rm d})$ with 300 Hz span. (b) ESA measurement of current power spectrum from $f_{\rm rep}$ to $f_{\rm rep}+f_{\rm d}$. In (a) and (b), experimental $P(f_{\rm rep})$ and $P(f_{\rm rep}+\mathrm{f_d})$ values are compared to calculated results. (c) Maximum hold traces with 10% dithering and no dither, along with system noise floor. In all measurements, ESA resolution bandwidth of 3 Hz is used.

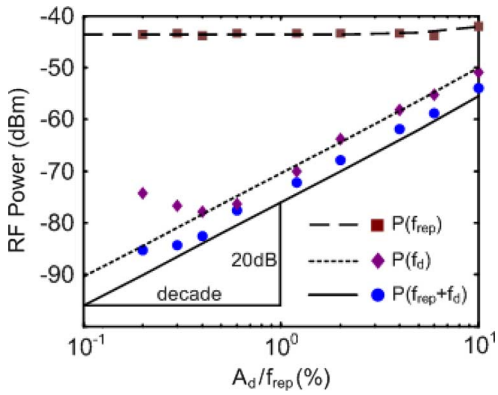

Fig. 8. Experimental (symbols) and theoretical (lines) values of $P(f_{\rm d})$, $P(f_{\rm rep})$, and $P(f_{\rm rep}+f_d)$ against $A_{\rm d}$ for single-line filtering.

in (10) and pointed out in subsequent discussion point 5), one should thus expect the dithering noise peak $f_{\rm rep}+f_{\rm d}$ to show the same line shape as the $f_{\rm rep}$ beat. This point is indeed justified within Fig. 7(b) and (c).

Fig. 8 shows the experimental results (symbols) of $P(f_{\rm d})$, $P(f_{\rm rep})$, and $P(f_{\rm rep}+f_{\rm d})$ values for various dithering amplitudes along with calculated results (lines) using our numerical method. For these data, the span of the ESA is 300 Hz with resolution bandwidth (RBW) of 3 Hz. Noise peak values are averaged from 20 acquisitions, each with a sweep time of 10 s.

Authorized licensed use limited to: Purdue University. Downloaded on October 15, 2009 at 10:49 from IEEE Xplore. Restrictions apply.

TABLE I

EXPERIMENTAL AND CALCULATED NOISE PEAK VALUES FOR TWO-LINE FILTERING AT $2f_{\rm rep}$ WITH $Ad/f_{\rm rep} = 10\%$. PHASE CONTROL OF $\Phi = \{\pi, \pi/2, \text{ and } 0\}$ ARE APPLIED TO LINE $\{-1\}$ FOR INVESTIGATION OF PHASE-SHAPING-CONTRIBUTED INTENSITY NOISE. THE CALCULATED PEAK VALUES ARE NORMALIZED TO THE EXPERIMENTAL $2f_{\rm rep}$ PEAK AND GIVEN IN dB. EXPERIMENTAL PEAKS ARE ACQUIRED USING ESA RESOLUTION BANDWIDTH OF 3 Hz. Δ_1, AND Δ_2 REPRESENT THE CONTRAST RATIOS BETWEEN THE PEAKS AT $f_{\rm rep}$ TO $f_{\rm rep} + f_{\rm d}$ AND $2f_{\rm rep}$ to $2f_{\rm rep} + f_{\rm d}$, RESPECTIVELY

	Peak frequency	f_d (dB)	f_{rep} (dB)	$f_{rep}+f_d$ (dB)	Δ_1 (dB)	$2f_{rep}$ (dB)	$2f_{rep}+f_d$ (dB)	Δ_2 (dB)
Φ=π	Data	-59.42	-39.51	-53.31	13.80	-27.52	-62.66	35.14
	Calculation	-59.80	-40.31	-54.45	14.14	-27.52	-63.21	35.69
Φ=π/2	Data	-60.50	-40.33	-56.82	16.49	-27.83	-63.15	35.32
	Calculation	-61.09	-40.96	-57.67	16.71	-27.83	-63.95	36.12
Φ=0	Data	-60.13	-48.66	-65.61	16.95	-27.62	-65.00	37.38
	Calculation	-60.74	-49.00	-66.65	17.65	-27.62	-65.31	37.69

Experimental results are in nice agreement to our calculations. We first note that $P(f_{\rm rep})$ remains nearly a constant throughout; thus, Δ_1 provides a direct measure of comb frequency dither amplitude. From the results of $P(f_{\rm d})$ and $P(f_{\rm rep} + f_d)$, experimental data are consistent with the 20 dB/decade relation, as anticipated for $A_{\rm d}/f_{\rm rep}$ above 0.4%. In our experiment, the effect of the comb frequency dithering can be directly discerned down to 36.6 MHz (0.4%) dither amplitude. From the 20 dB/decade scaling relation, we may extrapolate to predict the noise contribution from smaller frequency variations.

B. Two-Line Filtering at $2f_{\rm rep}$

In contrast to the single-line filtering case, where only intensity control is applied by the shaper, here we extend our investigation to the impact of frequency dithering on line-by-line $\{\text{intensity} + \text{phase}\}$ shaped waveforms. In this part, we show our experimental results with lines $\{-1 \text{ and } 1\}$ selected. In different experiments, the phase of line $\{-1\}$ is controlled by the line-by-line shaper with values $\Phi = \{\pi, \pi/2, 0\}$. Measurement settings are the same as for the single-line filtering case, but with an input average optical power of 1.0 dBm into the photodetector. To better prove the validity of our theoretical model, Table I summarizes the experimental and calculated noise peak values, with a dithering amplitude of 10%. Calculated peak values are normalized to the experimental peak value at $2f_{\rm rep}$. Excellent agreement is reached between the three experimental and calculated data sets. The peaks at frequencies $\{f_{\rm d}, f_{\rm rep}, f_{\rm rep} + f_{\rm d}, 2f_{\rm rep}, \text{ and } 2f_{\rm rep} + f_{\rm d}\}$ are given. Δ_1, and Δ_2 denote the contrast ratios between the peaks at $f_{\rm rep}$ to $f_{\rm rep} + f_{\rm d}$ and $2f_{\rm rep}$ to $2f_{\rm rep} + f_{\rm d}$, respectively.

Using the results shown in Table I, we observe the following: from the contrast ratios $\{\Delta_1, \Delta_2\}$, one can grasp how susceptible the waveforms are to frequency dithering and to a good extent how the waveforms evolve. The larger the noise peaks and the smaller the contrast, the greater the impact the frequency dither has on that particular RF frequency component. For example, for all three phase values, Δ_2 is greater than 35 dB, while Δ_1 values are of the order of 13∼18 dB. The actual noise peak values at $f_{\rm rep} + f_{\rm d}$ vary by 12.30 dB as phase control value Φ is changed from π to 0. This indicates that the waveforms tend to undergo a repetition rate change from the initial $2f_{\rm rep}$ waveform to a $f_{\rm rep}$ waveform periodicity, with this tendency exhibited most strongly for $\Phi = \pi$ phase control. This can be attributed to the field contribution from line $\{0\}$, which participates in the waveform generation with a weighting that depends on the frequency dithering amplitude. This finding is consistent with our previous report [18]. It is evident that the phase control has significant impact on the RF peaks at $f_{\rm rep}$ and $f_{\rm rep} + f_{\rm d}$, but not on the other peaks (consistent with time-domain traces shown in Figs. 1 and 4). This is highlighted using the bold frame within Table I. These results are in good accord with the qualitative predictions provided by our time-domain picture in [2]. The linkage is elaborated in the following paragraph.

To support our arguments, Fig. 9 shows the experimental ESA measurements over frequency ranges $\{f_{\rm rep} \sim f_{\rm rep} + f_{\rm d}\}$ with 10% dithering amplitude for the three phase control values. Corresponding calculated intensities and the magnified intensity peaks with {0 (solid), 10 (dotted)}% static frequency shifts are plotted. From our time-domain picture (static shift analysis), we anticipate greater intensity variations (waveform noise) showing up at *T*/2 points compared to 0 and *T* points. From the figures showing the magnified peaks, this point is indeed well taken. The $\Phi = \pi$ case [Fig. 9(a)] shows the decreased peaks at odd multiples of *T*/2 but stationary peaks at 0 and *T*, contributing to a stronger $f_{\rm rep}$ RF component when dithering is on. Thus, the dithering result yields a largest noise peak value at $f_{\rm rep} + f_{\rm d}$, indicating that this waveform is most susceptible to frequency dither and the change in waveform is most sensitive in its $f_{\rm rep}$ RF component. For $\Phi = 0$ case [Fig. 9(c)], calculated intensity with 10% static frequency shift shows all the peaks are equally decreased, since the intensity peaks are displaced an equal distance between 0 and *T*/2. The $f_{\rm rep}$ RF harmonic of this waveform is therefore less prone to frequency dithering, so the noise peak at $f_{\rm rep} + f_{\rm d}$ is 12.30 dB less as compared to the $\Phi = \pi$ case.

The relationships of $P(f_{\rm rep} + f_{\rm d})$ against dithering amplitudes with different phase controls are conducted using the same method as for one-line filtering case, shown in Fig. 10(a). Experimental data are shown using symbols while calculated values are depicted using lines. The experimental data for both $\Phi = \{\pi \text{ and } \pi/2\}$ fit the 20 dB/decade scaling all the way down to 0.2% dither and show ∼3 dB difference caused by phase control. For $\Phi = 0$, the experimental data adhere to the theoretical line only between {1% and 10}% with a ∼13 dB difference compared to $\Phi = \pi$ case, but deviate from the ideal curve for smaller dithering amplitudes. This finding is confirmed with multiple attempts. Possible reason is that, for $\Phi = 0$ case, beat

Authorized licensed use limited to: Purdue University. Downloaded on October 15, 2009 at 10:49 from IEEE Xplore. Restrictions apply.

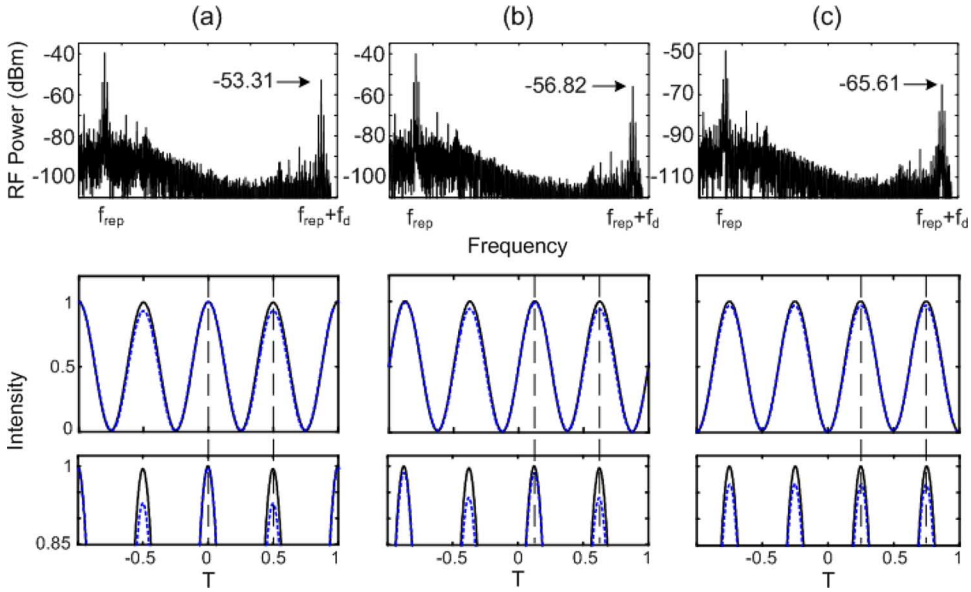

Fig. 9. Two-line filtering at $2f_{\rm rep}$ with $A_{\rm d}/f_{\rm rep} = 10\%$: Experimental ESA traces from $f_{\rm rep}$ to $f_{\rm rep} + f_{\rm d}$ with resolution bandwidth of 3 Hz. Phase control of $\Phi = \{\pi(\rm a), \pi/2(\rm b), \text{ and } 0(\rm c)\}$ is applied to line $\{-1\}$ for investigation of shaper-contributed intensity noise. Corresponding intensities with {0 (solid), 10 (dotted)}% static frequency shift and the expanded view on the intensity peaks are shown. As an aid to the eye, dashed lines denote the temporal positions as aid to the eye of peaks in the intensity waveforms.

signals are much lower than the other two phase values, leading to more vulnerability to system limitations. For $\Phi = \pi$ and $\pi/2$ cases, the achieved sensitivity of 0.2% is better than the single-line filtering case. Note that the waveform design with $\Phi = \pi$ (corresponding to the proposed waveform shown in Fig. 1(d), with π intrinsic phase of line $\{-1\}$ compensated by the shaper) is predicted to yield high sensitivity for monitoring of frequency fluctuations [18]. This is verified by our experiments. Using the definition in (13) and our data values, we can obtain $\eta_{1,2}$ of $\{-205.02, -208.21, -217.22\}$ (dBc/Hz) and $\eta_{2,2}$ of $\{-214.37, -214.55, -216.61\}$ (dBc/Hz) for phase values $\Phi = \{\pi, \pi/2, 0\}$, respectively.

Now, we investigate the effect when a static comb frequency bias $\varepsilon_{\rm b}$ is provided. Comb line frequencies relative to the filter function are now

$$\widetilde{f}_m = (m - m')f_{\rm rep} + \varepsilon_b + \delta\varepsilon(t) \tag{18}$$

where $m'\rm f_{rep}$ denotes the frequency of PMCW comb line $\{0\}$ that is aligned to the center of the shaper filter function. In practice, $\varepsilon_{\rm b}$ is provided by mounting the LCM on a translational stage and shifting it (and thus, the filter function) perpendicular to the optical axis.

Fig. 10(b) shows the relationship of $P(f_{\rm rep} + f_{\rm d})$ against different A_d using two-line filtering with $\Phi = \pi$ applied to line $\{-1\}$ as an example. Experimental data are shown with symbols for $\varepsilon_{\rm b}$ of {0%, 20%, and 30}% along with theoretical values shown using lines. All experimental data show a 20 dB/decade relation to varying $A_{\rm d}$. $P(f_{\rm rep} + f_{\rm d})$ is offset vertically by 5.5 and 9.6 dB for bias values of 20% and 30%, respectively, relative to the case of zero bias. With a 30% frequency bias, our data match the simulation results down to 0.12% frequency dither (10.98 MHz). For this example, we note the much improved sensitivity to offset frequency variations (by ~50 times) as compared to our previous static offset analysis, where we used sampling scope data to discern the effect of frequency shifts of roughly 500 MHz and above [18].

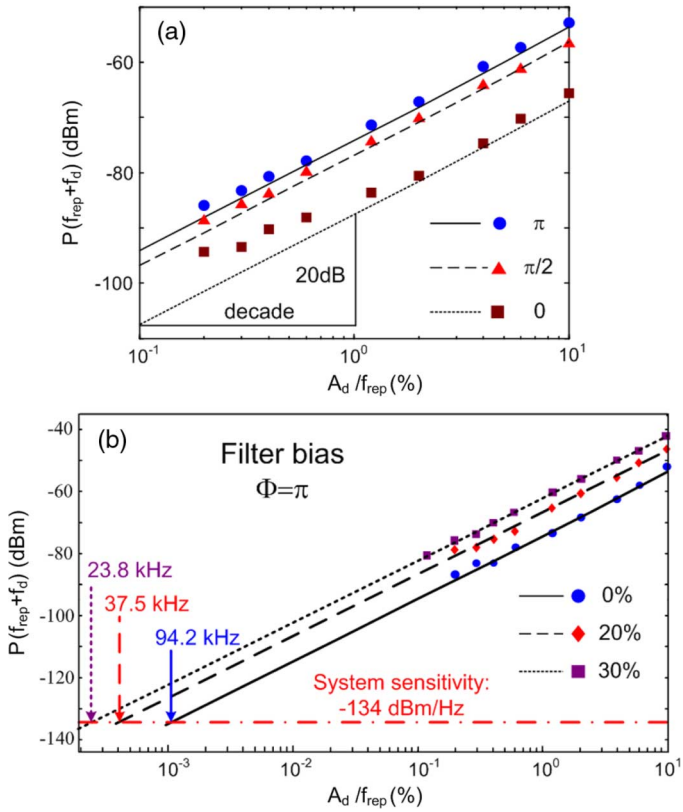

Fig. 10. Experimental results of $P(f_{\rm rep} + f_{\rm d})$ against $A_{\rm d}$ for two-line filtering at $2f_{\rm rep}$. (a) Data are shown with symbols for phase control values $\Phi = \{\pi, \pi/2, \text{ and } 0\}$ along with theoretical values shown using lines. (b) Filter frequency bias results with $\Phi = \pi$. Experimental data are shown with symbols for bias positions of {0%, 20%, and 30%} along with theoretical results shown using lines. Extrapolations of the 20 dB/decade scaling relation to the system sensitivity (dash-dotted line) are also used to find the shaper tolerance to laser linewidth.

Authorized licensed use limited to: Purdue University. Downloaded on October 15, 2009 at 10:49 from IEEE Xplore. Restrictions apply.

TABLE II
LIST OF NOISE PEAKS WITH 10% DITHERING AMPLITUDE FOR MINIMUM SPOT RADIUS $w_o = \{95, 70 \text{ and } 40\}$ μm AND EXTINCTION RATIO (ER) OF {20, 40} dB TO LINE {0}

w_0 (μm)	ER (dB)	P(f_d)	P(f_{rep})	P(f_{rep}+f_d)	P(2f_{rep})	P(2f_{rep}+f_d)
95	20	-59.80	-40.31	-54.45	-27.52	-63.21
	40	-71.94	-59.41	-54.35	-27.48	-86.39
70	20	-74.53	-40.26	-67.87	-27.44	-76.40
	40	-92.48	-60.14	-67.82	-27.38	-96.81
40	20	-128.24	-40.21	-121.04	-27.32	-129.54
	40	-148.23	-60.21	-120.99	-27.31	-149.54

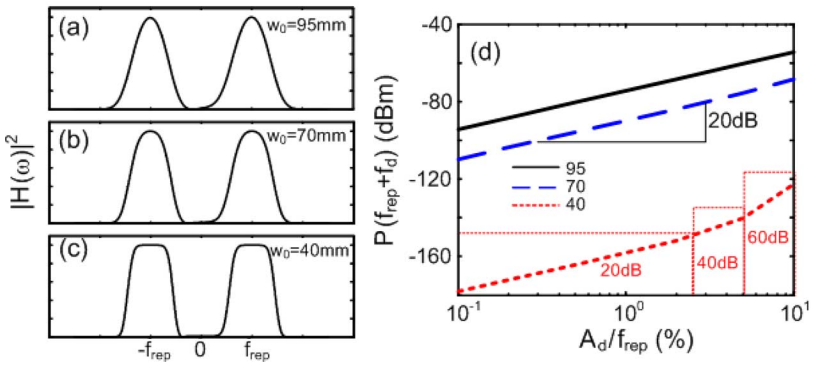

Fig. 11. Effects of shaper parameters on frequency dither noise through simulation: using 2-line filtering at $2f_{\text{rep}}$ with $\Phi = \pi$ case as example. LCM pixel size of 100 μm is fixed. (a)–(c) $|H(\omega)^2|$ for the three radii with ER = 20 dB. (d) $P(f_{\text{rep}} + f_{\text{d}})$ against dithering amplitude for $w_o = \{95\,(\text{solid}), 70\,(\text{dashed}), \text{ and } 40\,(\text{dotted})\}$ μm.

In Fig. 10(b), we have extended the theoretical calculations (lines) for each of the three bias values down to our current system sensitivity of -134 dBm/Hz, shown as the dash-dotted line, by using the 20 dB/decade scaling relation. The intersections give the minimum linewidths for which shaping intensity noise induced by frequency dither is above the measurement sensitivity. For these examples the minimum linewidths are {94.2, 37.5, and 23.8} kHz for {0, 20, and 30}% comb frequency bias shifts, respectively. These minimum linewidth values provide another metric of pulse shaping sensitivity to frequency fluctuations. We note that this sensitivity varies from waveform to waveform. However, our approach identifies a metric that can be used to compare the sensitivity to frequency noise to intensity noise conversion for different waveforms in line-by-line shaping.

VI. EFFECT OF SHAPER PARAMETERS

In this part, we use our numerical simulation method to explore how shaper parameters affect sensitivity to frequency dithering. The shaper parameters under concern are power extinction ratio and shaper spectral resolution. As shown in (2), finite extinction ratio is incorporated through nonzero $M(x)$; while shaper spectral resolution is dominated by the minimum spot radius w_0 at the focal plane. Better spectral resolution is achieved by having smaller w_0.

We choose the case of 2-line filtering with $\Phi = \pi$ for our discussion. Here, the pixel spacing is kept fixed at 100 μm (conforming to the LCM we are using) while w_0 is varied. Table II lists the noise peak values with 10% dithering amplitude, $w_0 = \{95, 70, \text{ and } 40\}$ μm and an extinction ratio of 20 and 40 dB for line {0}, respectively. With a better extinction ratio (40 dB), the harmonic peak at f_{rep} is suppressed by $\sim$20 dB, providing higher waveform fidelity. For better resolution (smaller w_0), dither-induced noise peaks at f_{d}, $f_{\text{rep}} + f_{\text{d}}$, and $2f_{\text{rep}} + f_{\text{d}}$ are reduced, but harmonic peaks at f_{rep} and $2f_{\text{rep}}$ are unaltered. These aspects can be understood from the $|H(\omega)|^2$ for the three radii shown in Fig. 11(a)–(c). With a smaller w_0, the resulting $|H(\omega)|^2$ more closely resembles the rectangular mask function $M(x)$ defined by the LCM [18]. The resulting wider, flatter passband makes the shaped waveform less vulnerable to frequency dithering, at least for small dither amplitudes. Also, for smaller w_0 the edges of the pulse shaper transmission bands grow sharper. For sufficiently large dither amplitudes, these sharp transmission edges begin to be felt. The effect may be seen in Fig. 11(d), which shows simulated noise peak amplitudes $P(f_{\text{rep}} + f_{\text{d}})$ against dithering amplitude for the three radii values. For $w_0 = \{95 \text{ and } 70\}$ μm, $\text{P}(\text{f}_{\text{rep}} + \text{f}_{\text{d}})$ adhere to the 20 dB/decade relation. However, for $w_0 = 40$ μm the slope gradually changes with increasing dither amplitude from 20 dB (<2.5% dither amplitude) to 40 dB (2.5% to 5%) to 60 dB (>5%).

These results reveal better extinction ratio and finer spectral resolution are favored in line-by-line shaping, at least in the situation considered here where spectral masking is performed with a pixelated spatial light modulator with close to 100% fill factor. Smaller beam radius (better spectral resolution) makes waveforms less sensitive to frequency fluctuations, at least in most cases of practical interest where frequency fluctuations will be relatively small compared to comb spacing.

VII. CONCLUSION

In summary, we have demonstrated the first quantitative investigation of noise introduced by small time-varying optical comb frequency offsets into waveforms generated via line-by-

Authorized licensed use limited to: Purdue University. Downloaded on October 15, 2009 at 10:49 from IEEE Xplore. Restrictions apply.

line pulse shaping. Deterministic variations of the offset frequency are obtained by frequency dithering of a continuous-wave laser that is fed into a phase modulator. This results in a controllable effective linewidth broadening. An electrical spectrum analyzer is used to examine the current power spectra of time-domain intensity waveforms subject to frequency dithering of the input. A theoretical model predicting a 20 dB/decade scaling relation between the fundamental dither-induced noise peak and the frequency dither amplitude is presented. A numerical simulation method capable of predicting the precise form of the RF power spectrum in the presence of optical frequency dithering is explained. Two specific simple examples of line-by-line shaping, where either a single line or a pair of lines are selected from the comb, are considered in detail. Experimental data are in excellent agreement with the simulated results down to frequency dithers of a few tenths of a percent (a few tens of megahertz, since the comb line frequency spacing is 9.15 GHz), more than an order of magnitude improvement in sensitivity as compared to our previous report. Our results may also be used to predict the contribution of offset frequency variations to pulse shaping noise even for smaller frequency variations. Furthermore, our approach shows how to calculate the proportionality between the variance of the frequency fluctuations and the resulting time-domain waveform variance for general frequency fluctuation noise spectra.

It is worth noting that the amplitude of pulse shaping intensity noise induced by a certain level of offset frequency fluctuations depends on the specific pulse shaping filter function. This, in turn, depends both on the masking function programmed into the pulse shaper and the spectral resolution of the pulse shaper optics. Here, for the most part, we looked at results for a pulse shaper using a spatial light modulator made of pixels with $\sim$100% fill factor and with pixel spacing corresponding to 4.575 GHz at a 2.6 GHz optics-limited spectral resolution, corresponding to the parameters of our line-by-line pulse shaping experimental apparatus. The effect of different pulse shaper spectral resolutions was explored through simulation. Within the parameter range considered, improved spectral resolution reduces waveform noise induced from optical frequency fluctuations.

REFERENCES

[1] A. M. Weiner, "Femtosecond pulse shaping using spatial light modulators," *Rev. Sci. Instrum.*, vol. 71, no. 5, pp. 1929–1960, May 2000.

[2] Z. Jiang, D. S. Seo, D. E. Leaird, and A. M. Weiner, "Spectral line-by-line pulse shaping," *Opt. Lett.*, vol. 30, no. 12, pp. 1557–1559, Jun. 2005.

[3] Z. Jiang, C.-B. Huang, D. E. Leaird, and A. M. Weiner, "Optical arbitrary waveform processing of more than 100 spectral comb lines," *Nat. Photon.*, vol. 1, no. 8, pp. 463–467, Aug. 2007.

[4] T. Udem, R. Holzwarth, and T. W. Hansch, "Optical frequency metrology," *Nature*, vol. 416, pp. 233–237, Mar. 2002.

[5] S. T. Cundiff, "Phase stabilization of ultrashort optical pulses," *J. Phys. D*, vol. 35, no. 8, pp. R43–R59, Apr. 2002.

[6] D. J. Jones, S. A. Diddams, J. K. Ranka, A. Stentz, R. S. Windeler, J. L. Hall, and S. T. Cundiff, "Carrier-envelope phase control of femtosecond mode-locked lasers and direct optical frequency synthesis," *Science*, vol. 288, pp. 635–639, Apr. 2000.

[7] S. Gee, F. Quinlan, S. Ozharar, and P. J. Delfyett, "Simultaneous optical comb frequency stabilization and super-mode noise suppression of harmonically mode-locked semiconductor ring laser using an intracavity etalon," *IEEE Photon. Technol. Lett.*, vol. 17, no. 1, pp. 199–201, Jan. 2005.

[8] M. Yoshida, T. Yaguchi, S. Harada, and M. Nakazawa, "A 40 GHz regeneratively and harmonically mode-locked erbium-doped fiber laser and its longitudinal-mode characteristics," *IEICE Trans. Electron.*, vol. E87C, no. 7, pp. 1166–1172, Jul. 2004.

[9] E. A. Avrutin, J. H. Marsh, and E. L. Portnoi, "Monolithic and multigigahertz mode-locked semiconductor lasers: Constructions, experiments, models and application," *IEE Proc. Optoelectron.*, vol. 147, no. 4, pp. 251–278, Aug. 2000..

[10] T. Kobayashi, H. Yao, K. Amano, Y. Fukushima, A. Morimoto, and T. Sueta, "Optical pulse compression using high-frequency electrooptic phase modulation," *IEEE J. Quantum Electron.*, vol. 24, no. 2, pp. 382–387, Feb. 1988.

[11] M. Kourogi, K. Nakagawa, and M. Ohtsu, "Wide-span optical frequency comb generator for accurate optical frequency difference measurement," *IEEE J. Quantum Electron.*, vol. 29, no. 10, pp. 2693–2701, Oct. 1993..

[12] H. Murata, A. Morimoto, T. Kobayashi, and S. Yamamoto, "Optical pulse generation by electrooptic-modulation method and its application to integrated ultrashort pulse generators," *IEEE J. Sel. Topics Quantum Electron.*, vol. 6, no. 6, pp. 1325–1331, Nov./Dec. 2000.

[13] D. Miyamoto, K. Mandai, T. Kurokawa, S. Takeda, T. Shioda, and H. Tsuda, "Waveform-controllable optical pulse generation using an optical pulse synthesizer," *IEEE Photon. Technol. Lett.*, vol. 18, no. 5, pp. 721–723, Mar. 2006.

[14] C.-B. Huang, Z. Jiang, D. E. Leaird, and A. M. Weiner, "High-rate femtosecond pulse generation via line-by-line processing of a phase-modulated CW laser frequency comb," *Electron. Lett.*, vol. 42, no. 19, pp. 1114–1115, Sep. 2006.

[15] Z. Jiang, D. E. Leaird, and A. M. Weiner, "Optical processing based on spectral line-by-line pulse shaping on a phase modulated CW laser," *IEEE J. Quantum Electron.*, vol. 42, no. 7, pp. 657–665, Jul. 2006.

[16] N. K. Fontaine, R. P. Scott, J. Cao, A. Karalar, K. Okamoto, J. P. Heritage, B. H. Kolner, and S. J. B. Yoo, "32 phase $\times$ 32 amplitude optical arbitrary waveform generation," *Opt. Lett.*, vol. 32, no. 7, pp. 865–867, Apr. 2007.

[17] Z. Jiang, D. E. Leaird, C.-B. Huang, H. Miao, M. Kourogi, K. Imai, and A. M. Weiner, "Spectral line-by-line pulse shaping on an optical frequency comb generator," *IEEE J. Quantum Electron.*, vol. 43, no. 12, pp. 1163–1174, Dec. 2007.

[18] C.-B. Huang, Z. Jiang, D. E. Leaird, and A. M. Weiner, "The impact of optical comb stability on waveforms generated via spectral line-by-line pulse shaping," *Opt. Express*, vol. 14, no. 26, pp. 13164–13176, Dec. 2006.

[19] M. J. Ablowitz, B. Ilan, and S. T. Cundiff, "Noise-induced linewidth in frequency combs," *Opt. Lett.*, vol. 31, no. 12, pp. 1875–1877, Jun. 2006.

[20] J. K. Wahlstrand, J. T. Willits, T. R. Schibli, C. R. Menyuk, and S. T. Cundiff, "Quantitative measurement of timing and phase dynamics in mode-locekd lasers," *Opt. Lett.*, vol. 32, no. 23, pp. 3426–3428, Dec. 2007.

[21] Z. Jiang, D. E. Leaird, and A. M. Weiner, "Optical arbitrary waveform generation and characterization using spectral line-by-line control," *J. Lightw. Technol.*, vol. 24, no. 7, pp. 2487–2494, Jul. 2006.

[22] D. M. Baney and W. V. Sorin, *Fiber Optics Test and Measurement*, D. Derickson, Ed. Englewood Cliffs, NJ: Prentice-Hall, 1998, pp. 169–219.

[23] D. von der Linde, "Characterization of the noise in continuously operating mode-locked lasers," *Appl. Phys. B*, vol. 39, pp. 201–217, 1986.

Chen-Bin Huang (M'99) received the B.S. degree in electrical engineering from National Tsing Hua University, in 1997, and the M.S. degree in electro-optical engineering from National Chiao Tung University in 1999, both in Hsinchu, Taiwan. He received the Ph.D. degree from the School of Electrical and Computer Engineering, Purdue University, West Lafayette, IN, in 2008.

He joined the Institute of Photonics Technologies, National Tsing Hua University in August 2008 as an Assistant Professor. His current research interests include focus on arbitrary optical/millimeter-wave waveform generation, nanophotonics, and frequency comb applications. From 1999 to 2003, he was with the Opto-Electronics and Systems Laboratories (OES), Industrial Technology Research Institute (ITRI), Taiwan, as a Research Engineer engaged in developing passive fiber optical and photonic crystal devices.

Dr. Huang was the recipient of the Master's Thesis of the Year Award from the Optical Engineering Society of Republic of China in 1999, Personal Research Achievement Award by OES, and Personal Distinguished Research Achievement Award by ITRI, both in 2002. He received the Andrews and Mary I. Williams Fellowship at Purdue University, in 2004 and 2005. He was selected as a finalist for the LEOS 2007 Best Student Paper Award.

Authorized licensed use limited to: Purdue University. Downloaded on October 15, 2009 at 10:49 from IEEE Xplore. Restrictions apply.

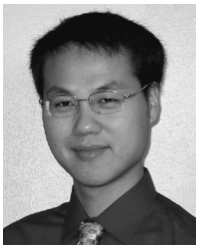

Zhi Jiang received the B.S. (highest honors) and M.S. degrees in electronics engineering from Tsinghua University, Beijing, China, in 1999 and 2002, respectively, and the Ph.D. degree in electrical and computer engineering from Purdue University, West Lafayette, IN, in 2006.

He is currently a Beckman Institute Postdoctoral Fellow, University of Illinois at Urbana-Champaign (UIUC), Urbana-Champaign. His research interests include biomedical optics, ultrafast optics and fiber optics.

Dr. Jiang received the Ross and Mary I. Williams Fellowship from Purdue University and the 2005 IEEE/LEOS Graduate Student Fellowship. He was selected as a finalist for the 2005 Optical Society of America (OSA) New Focus/Bookham Student Award and a finalist for the Purdue-Chorafas Best Thesis Award for the PhD thesis work. He was a recipient of the 2005 Chinese Government Award for Outstanding Graduate Students Abroad. In 2007, he was selected as one of the four recipients of the Beckman Postdoctoral Fellowship.

Daniel E. Leaird (M'01–SM'05) was born in Muncie, IN, in 1964. He received the B.S. degree in physics from Ball State University, Muncie, in 1987, and the M.S. and Ph.D. degrees from the School of Electrical and Computer Engineering, Purdue University, West Lafayette, IN, in 1996 and 2000, respectively.

He joined Bell Communications Research (Bellcore), Red Bank, NJ, as a Senior Staff Technologist in 1987, and later advanced to Member of Technical Staff. From 1987 to 1994, he was with the Ultrafast Optics and Optical Signal Processing Research Group, where he was a key team member in research projects in ultrafast optics, such as shaping of short optical pulses using liquid crystal modulator arrays, investigation of dark soliton propagation in optical fibers, impulsive stimulated Raman scattering in molecular crystals, and all-optical switching. He is currently a Senior Research Scientist and Laboratory Manager of the Ultrafast Optics and Optical Fiber Communications Laboratory, School of Electrical and Computer Engineering, Purdue University, where he has been since 1994. He has coauthored approximately 80 journal articles, 100 conference proceedings, and has three issued U.S. patents.

Dr. Leaird is active in the optics community and professional organizations including the Optical Society of America and IEEE Lasers and Electro-Optics Society (LEOS) where he is the chair of the Ultrafast technical committee as well as serving as a consultant to venture capitalists by performing technical due diligence. He also serves as a frequent reviewer for *Optics Letters*, *Photonics Technology Letters*, *Applied Optics*, and the *Journal of the Optical Society of America B* in addition to serving on National Science Foundation review panels in the SBIR program. He has received several awards for his work in the ultrafast optics field including a Bellcore "Award of Excellence", a Magoon Award for outstanding teaching, and an Optical Society of America/New Focus Student Award.

Andrew M. Weiner (S'84–M'84–SM'91–F'95) received the Sc.D. degree from the Massachusetts Institute of Technology (MIT), Cambridge, in 1984.

He then joined Bellcore, first as a Member of Technical Staff and later as Manager of Ultrafast Optics and Optical Signal Processing Research. He moved to Purdue University, West Lafayette, IN, in 1992 and is currently the Scifres Distinguished Professor of Electrical and Computer Engineering. He is the author or coauthor of six published book chapters, over 200 journal articles, over 350 conference papers, including approximately 80 conference-invited talks, and has presented nearly 100 additional invited seminars at university, industry, and government organizations. He is holder of ten U.S. patents. His current research interests inlcude ultrafast optics signal processing and applications to high-speed optical communications and ultrawideband wireless. He is especially well known for his pioneering work in the field of femtosecond pulse shaping.

Prof. Weiner is a Fellow of the Optical Society of America and a member of the U.S. National Academy of Engineering.He has served as Co-Chair of the Conference on Lasers and Electro-optics and the International Conference on Ultrafast Phenomena and as Associate Editor of several journals. He has also served as Secretary/Treasurer of IEEE LEOS and as a Vice-President of the International Commission on Optics (ICO)He has received numerous awards for his research, including the Hertz Foundation Doctoral Thesis Prize in 1984, the Adolph Lomb Medal of the Optical Society of America in 1990, the Curtis McGraw Research Award of the American Society of Engineering Education in 1997, the International Commission on Optics Prize in 1997, and the Alexander von Humboldt Foundation Research Award for Senior U.S. Scientists 2000. He is a joint recipient, with J.P. Heritage, of the IEEE LEOS William Streifer Scientific Achievement Award in 1999 and the OSA R.W. Wood Prize in 2008 and has been recognized by Purdue University with the inaugural Research Excellence Award from the Schools of Engineering in 2003 and with the Provost's Outstanding Graduate Student Mentor Award in 2008.

Authorized licensed use limited to: Purdue University. Downloaded on October 15, 2009 at 10:49 from IEEE Xplore. Restrictions apply.